iScience

CellPress
OPEN ACCESS

Article

Protein profile of mouse endolymph suggests a role in controlling cochlear homeostasis

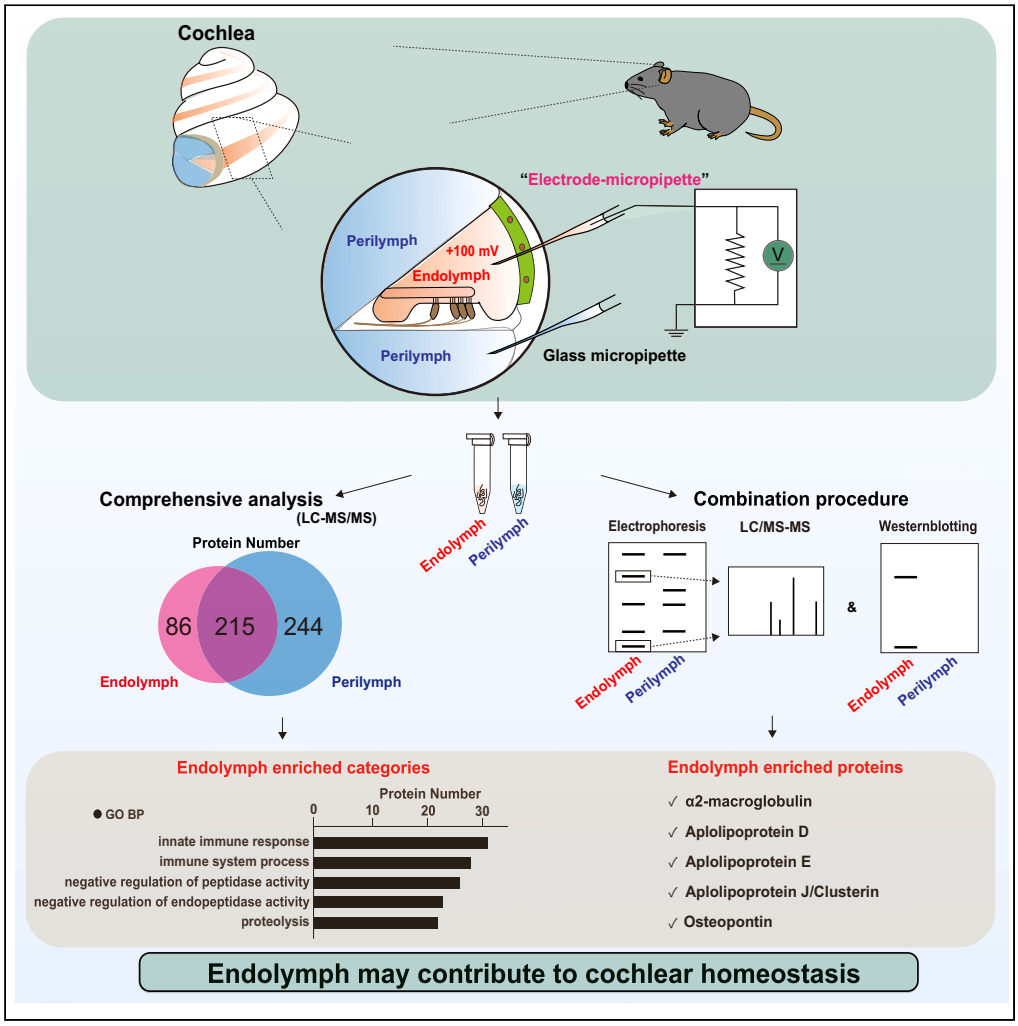

Masatoshi Fukuda, Hiroki Okanishi, Daisuke Ino, ..., Hidenori Inohara, Yoshikatsu Kanai, Hiroshi Hibino

hibino@pharma2.med.osaka-u.ac.jp

Highlights

A procedure for collecting endolymph from mouse cochleae was developed

Comprehensive analysis of the endolymph and perilymph revealed the protein profiles

Five proteins enriched in the endolymph were extracted by combining different methods

Endolymph may regulate cochlear homeostasis

Fukuda et al., iScience 27, 111214
November 15, 2024
https://doi.org/10.1016/j.isci.2024.111214

iScience

CellPress
OPEN ACCESS

Article

Protein profile of mouse endolymph suggests a role in controlling cochlear homeostasis

Masatoshi Fukuda,[1,2] Hiroki Okanishi,[3] Daisuke Ino,[1] Kazuya Ono,[1] Takeru Ota,[1] Eri Wakai,[1] Takashi Sato,[2] Yumi Ohta,[2] Yoshiaki Kikkawa,[4,5,6] Hidenori Inohara,[2] Yoshikatsu Kanai,[3,7,8] and Hiroshi Hibino[1,6,9,*]

SUMMARY

The cochlea contains two extracellular fluids, perilymph and endolymph. Endolymph exhibits high potential of approximately +80 to +110 mV (depending on species), which sensitizes sensory hair cells. Other properties of this unique fluid remain elusive, owing to its minuscule volume in rodent cochlea. We therefore developed a technique to collect high-purity endolymph from mouse cochleae. Comprehensive proteomic analysis of sampled endolymph using liquid chromatography with mass spectrometry identified 301 proteins, dominated by molecules engaged in immunity and proteostasis. Approximately 30% of these proteins were undetectable in our perilymph. A combination of mass spectrometry and different approaches revealed that, compared to perilymph, endolymph was enriched with α_2-macroglobulin, osteopontin, apolipoprotein D, apolipoprotein E, and apolipoprotein J/clusterin. In other cells or tissues, α_2-macroglobulin, apolipoprotein E, and apolipoprotein J contribute to the clearance of degraded proteins from extracellular fluid. Altogether, with the proteins described here, endolymph may play a protective role in stabilizing cochlear homeostasis.

INTRODUCTION

Hearing is essential for vertebrates. The mechanical energy of sound is converted into electrical signals by the cochlea of the inner ear (Figure 1A). This peripheral auditory organ comprises three tubular structures: the scala tympani, scala media, and scala vestibuli. Whereas the scala tympani and scala vestibuli are filled with perilymph, the scala media contains endolymph (Figures 1B and 1C). In adult rodents, the electrochemical characteristics of these two fluids are different. The ionic composition of the perilymph is similar to that of plasma, whereas the endolymph contains a high [K^+] of 150–200 mM and a low [Na^+] of ~3 mM.[1–5] Furthermore, the latter exhibits a highly positive electric potential, endocochlear potential (EP), of approximately +80 to +110 mV, relative to the perilymph.[2–8] Upon mechanical stimulation, K^+ in the endolymph enters the hair cells in the sensory epithelium and excites the cells. Positive EP accelerates K^+ influx, sensitizing hair cells.[9,10] The sensory epithelium also contains multiple supporting cell types that likely maintain the architecture of the epithelium and regulate the extracellular and intracellular ionic environments required for functioning hair cells.[11]

In humans, hearing loss or deafness not only dramatically reduces the quality of life but is also strongly associated with dementia.[12,13] Most types of irreversible hearing impairment result from cochlear dysfunction or injury with several different causes. Representative acquired factors include aging, acoustic trauma, and ototoxic drugs.[14–17] In congenital cases, a considerable number of mutations in genes encoding cytoskeletal, matrix, ion transport, receptor, and cell signaling proteins have been identified.[18–20] Such stresses affect sensory hair cells, supporting cells, and the extracellular matrix. Many cellular and tissue components in the cochlea are exposed to the endolymph (Figure 1C); therefore, this extracellular fluid may control the physiological state of the cochlea and may also be involved in pathophysiological processes. An approach to explore this possibility is to elucidate its repertoire of proteins. Mouse models are the most frequently used for studies on hearing loss and can represent hearing phenotypes similar to the patterns of patients' auditory thresholds in response to harmful or toxic stimuli.[21,22] However, the inner ear is encased by bones, and in the cochlea of mice, the endolymph volume is extremely small (0.2–0.8 μL), compared to the volume of the perilymph (0.6–1 μL).[23,24] Therefore, in this animal species, the property of the endolymph, other than its ionic milieu, has not yet been characterized, although one group reported limited information on the protein composition of this fluid in guinea pigs, which have a much larger inner ear volume than mice.[25,26]

[1]Division of Glocal Pharmacology, Department of Pharmacology, Graduate School of Medicine, Osaka University, 2-2 Yamadaoka, Suita, Osaka 565-0871, Japan
[2]Department of Otorhinolaryngology, Graduate School of Medicine, Osaka University, 2-2 Yamadaoka, Suita, Osaka 565-0871, Japan
[3]Department of Bio-system Pharmacology, Graduate School of Medicine, Osaka University, 2-2 Yamadaoka, Suita, Osaka 565-0871, Japan
[4]Deafness Project, Department of Basic Medical Sciences, Tokyo Metropolitan Institute of Medical Science, Tokyo 156-8506, Japan
[5]Graduate School of Medical and Dental Sciences, Niigata University, Niigata 951-8510, Japan
[6]AMED-CREST, AMED, Osaka 565-0871, Japan
[7]Institute for Open and Transdisciplinary Research Initiatives, Osaka 565-0871, Japan
[8]Premium Research Institute for Human Metaverse Medicine (WPI-PRIMe), Osaka 565-0871, Japan
[9]Lead contact
*Correspondence: hibino@pharma2.med.osaka-u.ac.jp
https://doi.org/10.1016/j.isci.2024.111214

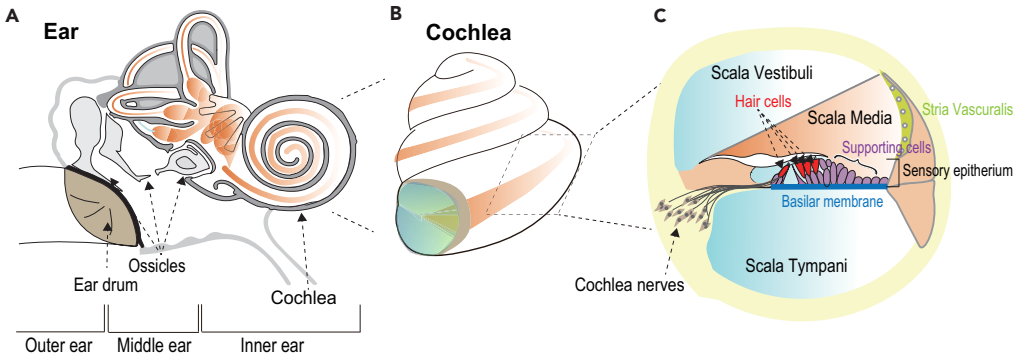

Figure 1. Structure and composition of the auditory organ in mammals

(A) Diagram of the ear. The organ consists of the outer, middle, and inner ears; the major components are shown in the panel.

(B and C) Structure of the cochlea. The outline and cross section are illustrated in (B) and (C), respectively. The cochlea is composed of three tubules: the scala vestibuli, the scala media, and the scala tympani (C). The scala media is filled with endolymph, whereas the other tubules contain perilymph. The tissue and cellular components inside the cochlea are shown in (C). In all panels, the endolymphatic spaces are highlighted in *brown*.

In this study, we therefore developed a technique to collect endolymph from mouse cochleae. A single-barreled needle-type micropipette, which was fabricated by filling the tip with a conductive organic solvent,[27] precisely identified the scala media containing the endolymph by monitoring its potential and succeeded in sampling a volume of the fluid of ~0.3 μL at maximum from a cochlea. Comprehensive proteomic analysis of the endolymph and perilymph samples revealed 301 and 459 proteins, respectively. The endolymph contains abundant molecules involved in the immune system and regulation of protein digestion. Of the proteins identified, 86 molecules were unique to the endolymph, suggesting that this fluid plays roles distinct from those of the perilymph. Further comparison of the protein composition of the two fluids by another approach unveiled enrichment of α_2-macroglobulin (A2M), osteopontin (OPN), apolipoprotein D (APOD), apolipoprotein E (APOE), and apolipoprotein J/clusterin (APOJ/CLN), in the endolymph. In particular, A2M, APOE, and APOJ/CLN likely remove degraded and denatured proteins from the extracellular fluid in the brain or in an *in vitro* system using cultured cells.[28–32] Collectively, the endolymph may protect fluid and cochlear cells with a unique array of proteins to maintain hearing. Our results provide an approach to not only elucidate the detailed processes for operating on the cochlea but also explore the pathophysiological mechanisms that underlie hearing loss.

RESULTS

Comprehensive analysis and characterization of proteins in mouse endolymph

In the mouse cochlea, we attempted to precisely determine the location of the scala media (Figure 1C) by detecting the high potential (~+100 mV) of the endolymph and collect as pure a fluid as possible from it. For this purpose, we fabricated a single-barreled needle-type "electrode micropipette," the tip of which was filled with a conductive organic solvent, tetradodecylammonium tetrakis 4-chlorophenyl borate (TDATPBCL; 10 mM) dissolved in 1,2-dichloroethane solution (Figure 2A). During each series of animal experiments, this micropipette, which was also subjected to sample an aliquot of endolymph, was connected to an electrometer for continuous monitoring of the potential (Figure 2B; see STAR Methods). Figure 2C shows electrical recording in a representative experiment using the cochlea of a live mouse. Upon insertion of an electrode micropipette from the perilymph in the lateral wall toward the scala media, potential was abruptly elevated to +109 mV, a hallmark of endolymph. In this passage, the contamination of the perilymph should be minimal owing to the hydrophobicity of TDATPBCL. While the electrode micropipette was held in the scala media, an aliquot of the endolymph was collected through the application of mechanical pressure. Finally, the pipette was removed from the cochlea. In this trial, ~0.2 μL of the fluid was obtained (Figure 2D).

Endolymph aliquots from 12 to 15 cochleae were homogenized and ~0.9 μg protein was subjected to the following experiments for each series of comprehensive analysis. First, the samples were analyzed using a proteomics approach with liquid chromatography-tandem mass spectrometry (LC-MS/MS). In total, 301 proteins were identified (Table S1). Using the Gene Ontology (GO) database, these proteins were classified based on their biological processes (BP) and cellular components (CCs) (Figure 2E). In the BP domain, "innate immune response" and "immune system processes" were the two most frequent categories of proteins, with 31 and 28 molecules, respectively (enrichment score: p = 1.6E−06 and 1.9E−07). These two categories contain different complement components: C1qb, C1ra, C2, C3, C8a, C8b, C8g, and C9. This lineup includes key proteins involved in classical, alternative, and lectin pathways in the complement system.[33] Notably, the categories of "negative regulation of peptidase activity," "negative regulation of endopeptidase activity," and "proteolysis" were third-, fifth-, and sixth-most abundant (26, 23, and 22 proteins; p = 1.4E−20, 5.2E−21, and 4.9E−04; respectively). This observation suggests that the endolymph controls protein digestion. A considerable number of the proteins belonged to the roles of cellular and tissue housekeeping annotations, such as "cell adhesion," "positive regulation of gene expression," and "intermediate filament organization" (23, 19, and 17 proteins; p = 9.2E−05, 7.4E−03, and 9.6E−15; respectively). Additionally, 18 proteins were annotated as "blood coagulation" (p = 9.6E−15), reminiscent of a function of blood plasma. From a CC standpoint, expectedly, the most abundant proteins were extracellular proteins, classified as

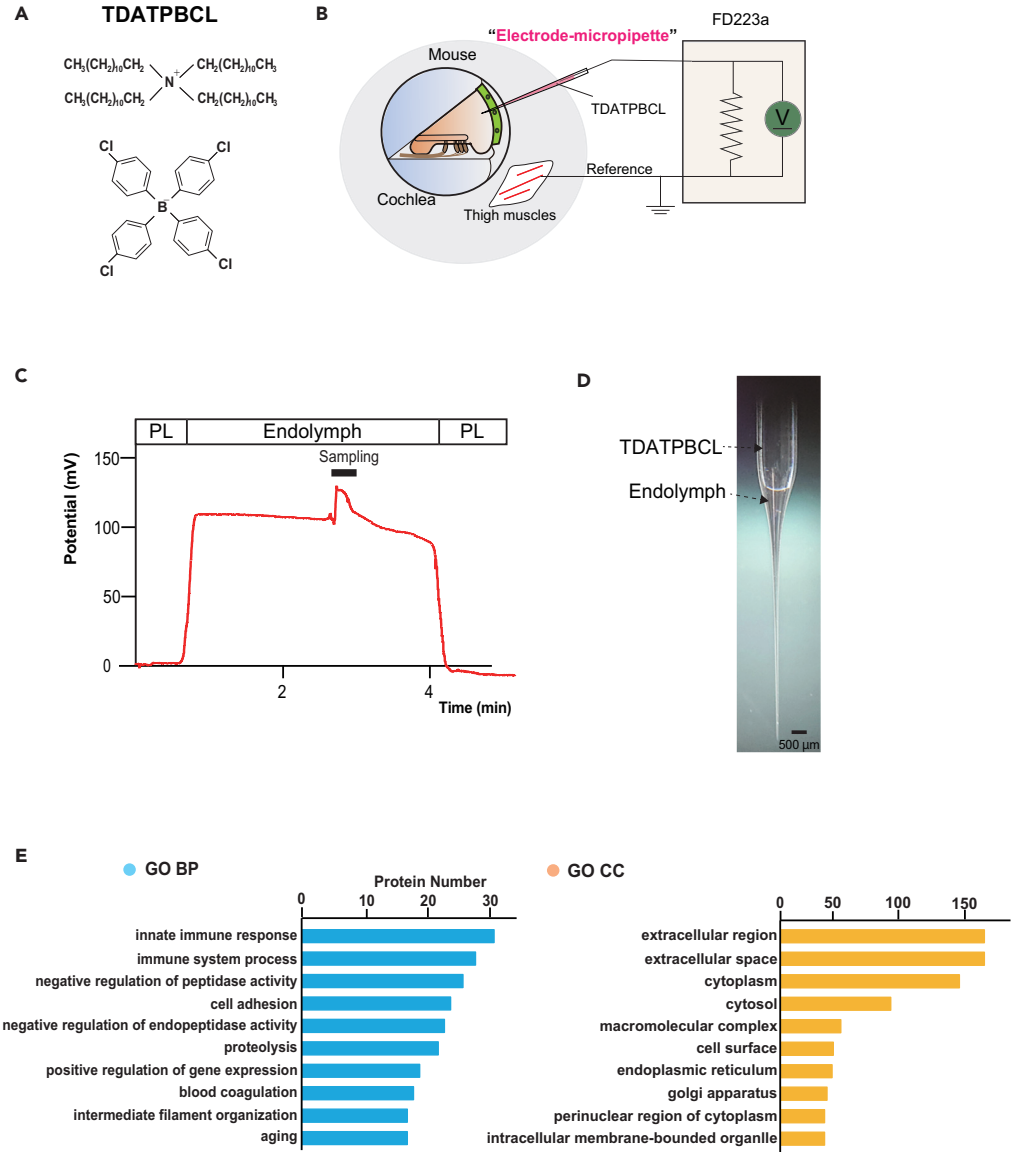

Figure 2. Sampling and proteomic analysis of mouse endolymph

(A) Structural formula of tetradodecylammonium tetrakis 4-chlorophenyl borate (TDATPBCL).

(B) Diagram for the circuit of the electrochemical cell used in the experiments for collecting endolymph. An "electrode micropipette," which was used for both sampling and continuous monitoring of the potential, was connected to a voltmeter, FD223a, in advance and inserted into the scala media of a mouse cochlea. A reference electrode was set to a muscle of the quadriceps femoris.

(C) Recording of the potential with an electrode micropipette in a mouse cochlea. A needle-type electrode micropipette fabricated using TDATPBCL (A) as described in the STAR Methods was inserted from the perilymph (PL) in the lateral cochlear wall to the endolymph. The endolymph in the scala media was marked by a highly positive potential of +109 mV, i.e., the endocochlear potential. At the timing of fluctuation of the potential, a small aliquot of the endolymph was sampled using an electrode micropipette by mechanical aspiration. Finally, the electrode micropipette was pulled back into perilymph.

(D) Endolymph collected in an electrode micropipette. In this case, the sample volume was estimated to be approximately 0.2 µL.

(E) Proteomic profile of the mouse endolymph. A sample (0.9 µg) gathering aliquots of endolymph from multiple cochleae was analyzed by LC-MS/MS (for the preparation, see "STAR Methods"). A total of 301 identified proteins were subjected to Gene Ontology (GO) analysis and the enriched proteins were classified based on biological processes (BP; *blue bars*) or cellular components (CCs; *yellow bars*). All protein annotations were presented in Table S1. In each domain, the top ten ranked categories with respect to the number of proteins are displayed.

extracellular regions (p = 1.2E−85) or extracellular spaces (p = 1.3E−80) (189 proteins for both). Nevertheless, nearly half of the endolymph proteins were characterized by the localization of "cytoplasm" or "cytosol" (p = 6.4E−4) (143 molecules), followed by annotations of six intracellular compartments, including cell surface (p = 9.3E−12) and organelles (p = 9.4E−4).

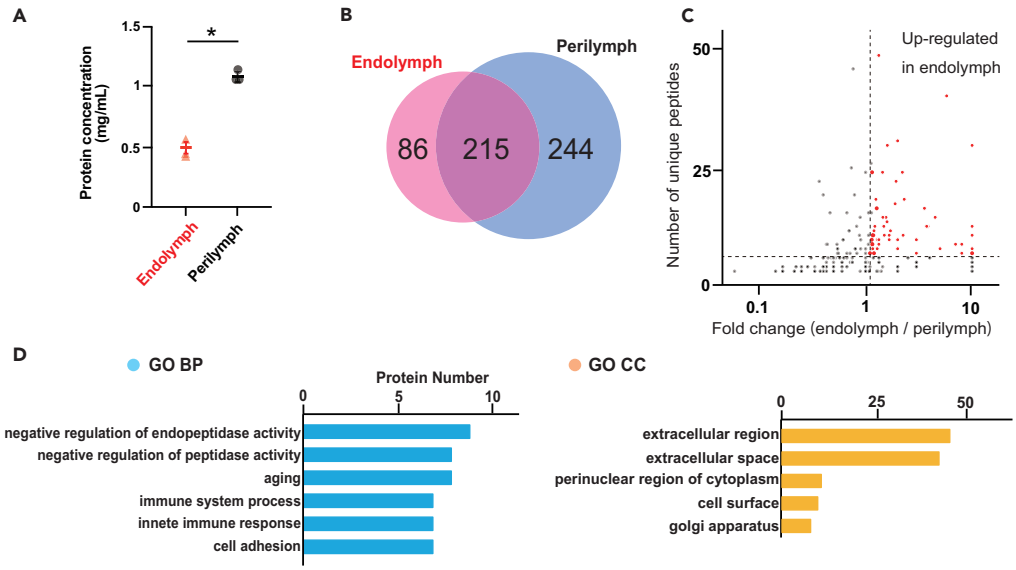

Figure 3. Comparison of protein contents between endolymph and perilymph

(A) Protein concentration. Three samples for each endolymph and perilymph were analyzed (for sample preparation, see "STAR Methods"); all the measurements are plotted with mean ± SD (*error bars*). *Asterisks* indicate significant differences: two-tailed Student's t test; $p = 5.1E{-}4$.

(B) Number of proteins identified in the two lymph fluids. A total of 301 proteins identified in the endolymph analysis related to Figure 2D and Table S1 were compared with 459 proteins extracted from a perilymph sample, as shown in Table S2; 215 proteins overlapped.

(C and D) Characterization of endolymph proteins. In (C), all 301 proteins identified in the endolymph are plotted against fold change (endolymph/perilymph) and the number of unique peptides detected by mass spectrometry and used for annotation of the endolymph proteins. A total of 56 proteins, indicated by *red dots*, satisfied the criteria of number of unique peptides ≥5 and fold change ≥1.1. The x axis is a logarithmic scale. Proteins whose peptides were identified exclusively in the endolymph but not in the perilymph were plotted along the axis of fold change = 10. These 56 proteins were further analyzed with Gene Ontology (GO) in terms of enrichment analysis in biological processes (BP) and cellular components (CCs), and the top-ranked six and five categories with the number of proteins are displayed in (D).

Comparison of protein profile between the endolymph and perilymph

Next, we compared the protein landscape of endolymph with that of perilymph (Figure 3). In mice, the concentration of endolymph was 0.50 ± 0.09 mg/mL ($n = 3$), which was roughly half that of perilymph (1.10 ± 0.06 mg/mL; $n = 3$) (Figure 3A). We further aimed to determine the differences in the protein composition between the two fluids. Comprehensive proteomic analysis of the perilymph using LC-MS/MS identified 459 proteins (Table S2). Using the GO algorithm, the perilymph proteins in the BP domain were characterized by immune response, control of protein degradation, and lipid metabolism, whereas those in the CC domain were categorized primarily into intracellular compartments with a certain number of annotations of extracellular localization (Figure S1). Of the 301 proteins present in the endolymph, 215 were detected in the perilymph dataset (Figure 3B). In Figure 3C, all proteins identified in the endolymph are plotted in terms of the spectral counting ratio relative to the perilymph (i.e., endolymph/perilymph) and the number of unique peptides that were detected in MS data and used for protein name annotation. When the thresholds of the two indices were set to ≥5 and ≥1.1, respectively, 56 proteins were extracted (Table S3). In other words, the expression of these proteins was ensured in the endolymph and was significantly more abundant than in the perilymph. These 56 proteins were analyzed using the GO algorithm (Figure 3D). In the BP domain, the top-ranked categories were engaged in the control of protein degradation, that is "negative regulation of endopeptidase activity" ($p = 8.9E{-}4$) and "negative regulation of peptidase activity" ($p = 1.1E{-}7$) (nine and eight molecules, respectively). The second highlighted annotations were related to immunity, such as "innate immune response" ($p = 4.4E{-}4$) and "immune system process" ($p = 4.8E{-}4$) (7 proteins for both). The latter includes complements C2, C8, and C9, suggesting that classical and lectin pathways are more active than alternative pathways in the endolymph.[33] These results indicate that compared to perilymph, the endolymph has a unique protein profile and likely plays different roles, highlighting the protection of the cochlear environment. It is reasonable that, in the CC domain, most of the common proteins were annotated by extracellular localization ("extracellular region" [$p = 6.7E{-}44$] [40 proteins] and "extracellular space" [$p = 3.3E{-}40$] [39 proteins]), whereas a limited number of proteins belonged to the intracellular compartments.

Proteins enriched in the endolymph

The detection sensitivity of MS is extremely high. In this context, we cannot rule out the possibility that a detected endolymph protein, when present in small quantities, could be attributed to contamination of the neighboring perilymph. Therefore, we used different approaches to determine the proteins that are definitively present in the endolymph and are also markedly enriched in this fluid compared to the perilymph (Figure 4). Initially, we analyzed endolymph and perilymph samples obtained from mouse cochleae using SDS-PAGE. When the

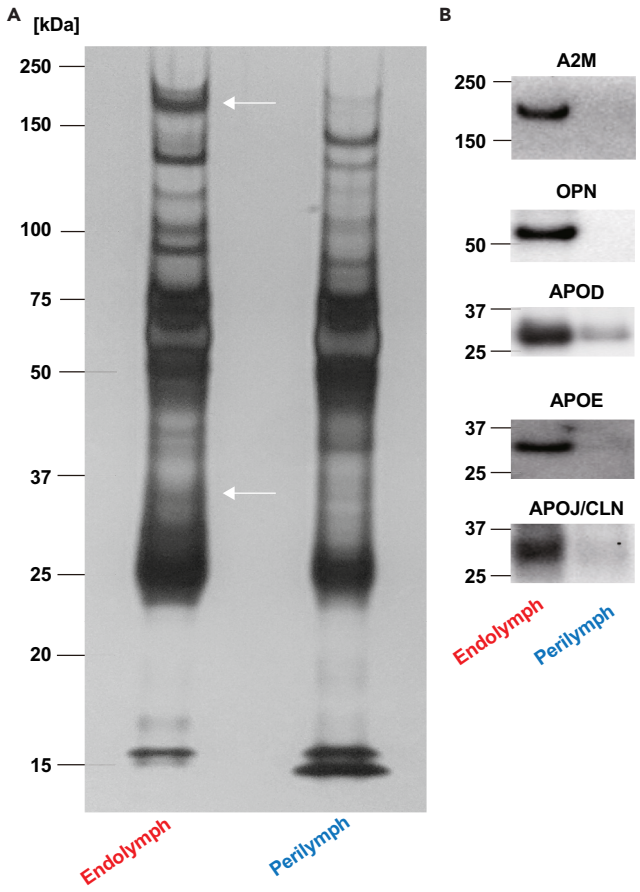

Figure 4. Biochemical characterization of mouse endolymph and perilymph

(A) Silver staining of endolymph and perilymph proteins analyzed by SDS-PAGE. 0.9 μg of the sample (for the preparation, see "STAR Methods") was applied to each lane. *Arrows* indicate bands likely to be unique to the endolymph. In this context, similar results were obtained for guinea pig samples (Figure S2).

(B) Western blot analysis. The membranes transferred with the samples of the two fluids (0.6 μg for each; see "STAR Methods" for sample preparation) were immunoblotted with antibodies against the molecules described above the panels. A2M, α_2-macroglobulin; OPN, osteopontin; APOD, apolipoprotein D; APOE, apolipoprotein E; APOJ/CLN, apolipoprotein J/clusterin.

polyacrylamide gel was subjected to silver staining, several protein bands were visible for each sample (Figure 4A). Careful observation revealed that the ~160 and ~35 kDa bands detected in the endolymph samples were, in contrast, negligible in the perilymph sample. Similar results were obtained when the guinea pig endolymph and perilymph were examined using the same methods (Figure S2). Accordingly, from the polyacrylamide gel analysis of endolymph and perilymph in mice (Figure 4A), the portions at ~160 and ~35 kDa in the two lanes were separately extracted, and the proteins in each of these four samples were subjected to LC-MS/MS. Based on the MS data (Tables S4 and S5) and a threshold criterion (see STAR Methods), we extracted the proteins that were more likely to be present in the endolymph than in the perilymph. With reference to molecular weight, A2M was a candidate for proteins with higher molecular mass, whereas OPN, APOD, APOE, and APOJ were likely included in proteins with lower molecular mass. The high enrichment of the five proteins in the endolymph was confirmed by western blotting using specific antibodies (Figure 4B). Notably, the signals of these proteins were negligible in perilymph samples. For technical evaluation, we attempted to examine whether the perilymph and endolymph samples contained sufficient albumin, because in LC-MS/MS analysis, this protein was characterized by the highest peptide spectrum match score for both samples (300 and 393 for endolymph and perilymph, respectively) (Figure 3C; Tables S1 and S2). When each immunoblotted membrane analyzed in Figure 4B was stripped and re-probed with an antibody against albumin, a clear band was indeed observed for each lymph sample (Figure S3A). Furthermore, in a different immunoblot experiment, a minimal signal was detectable in endolymph and perilymph samples with an antibody against β-actin, an indicator of cellular components (Figure S3B). The results of these evaluation experiments not only ensure the purity of the samples collected from the mouse cochlea but also support the reliability of our data that the five proteins are more abundant in the endolymph.

Expression and distribution of A2M in the mouse cochlea

Finally, we investigated whether the five enriched proteins in the endolymph were expressed in the cochlea. The data for OPN, APOD, APOE, and APOJ have been described in the literature as follows. The immunolabeling signal of APOD is detectable in the spiral ligament, stria

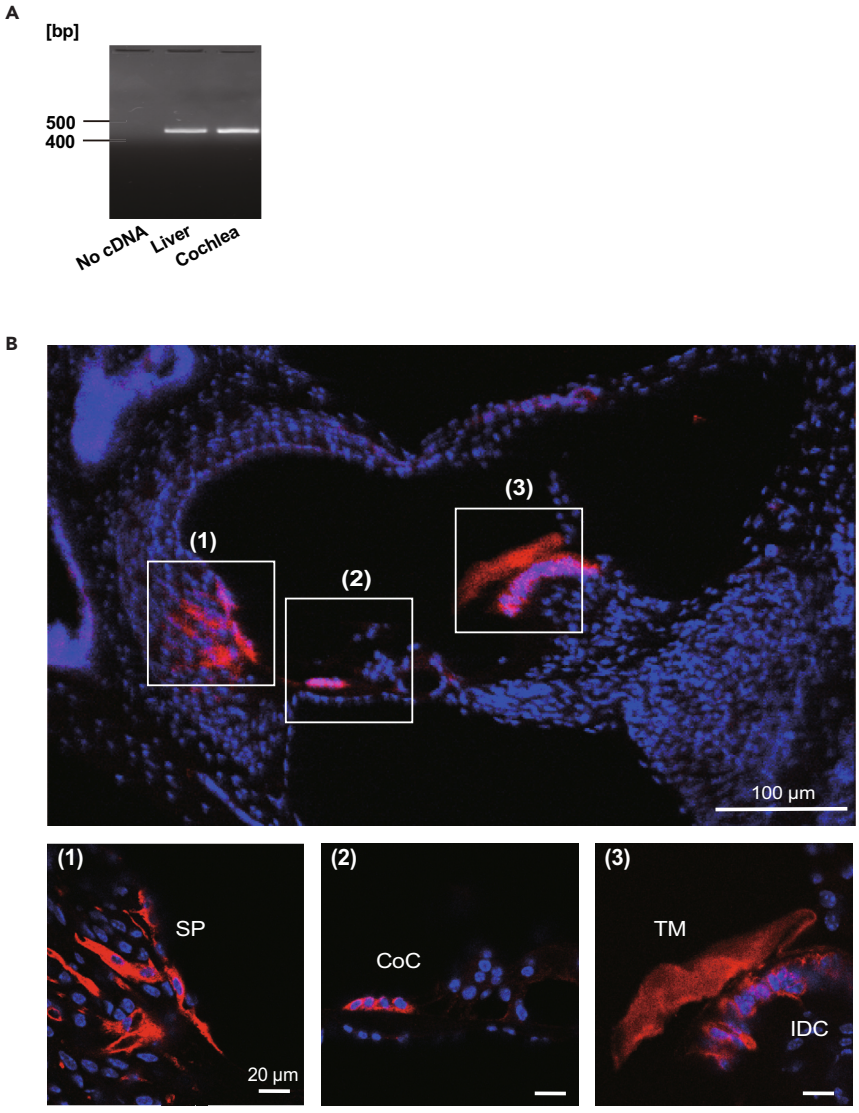

Figure 5. Expression and localization of A2M in the mouse cochlea

(A) Reverse-transcription PCR analysis of A2M. cDNA samples were synthesized from total RNAs isolated from the mouse liver and cochleae and amplified with a set of specific primers for *A2M*. A sample without cDNA was used for negative control experiment (labeled "*No cDNA*").

(B) Immunohistochemical preparation of mouse cochlea. In the low-magnification image (upper), an antibody specific to A2M markedly immunolabeled the tissue and cellular components in the *boxed* three regions. These regions are enlarged and displayed in the lower panels. A strong fluorescence signal was detected in the spiral-prominent (SP), Claudius cells (CoC), and internal interdental cells (IDCs). The signal detected in the tectorial membrane (TM) may represent a non-specific reaction.

vascularis, and hair cells of the cochlea.[34] Histochemically, OPN mRNA is present in strial marginal cells and spiral ganglia[35] whereas APOJ occurs in the outer hair cells, pillar cells, and Deiter's cells.[36] Single-cell RNA sequencing analysis revealed APOE transcription in outer hair cells, inner hair cells, Deiter's cells, and pillar cells.[37]

Neither the expression of A2M transcripts nor the cellular distribution of this protein has been examined in the rodent cochlea. Therefore, we conducted reverse-transcription PCR (RT-PCR) analysis using mouse cochlear total RNA (Figure 5A). A set of primers specific to *A2M* amplified a fragment at the expected base pairs from cochlear cDNA, as observed in the PCR product obtained from mouse liver RNA.[38] Moreover, immunolabeling of the mouse cochlea with an antibody specific to A2M showed strong signals in the interdental cells, Claudius cells, and outer sulcus cells in the spiral prominence (Figure 5B).

All cell types that express one or more protein(s) among the A2M, OPN, APOD, APOE, and APOJ are exposed to the endolymph. Accordingly, the five proteins enriched in the endolymph may be secreted from cells inside the cochlea, although the possibility that these proteins originate in other organs or blood cannot be ruled out.

DISCUSSION

In this study, we collected high-purity endolymph from mice using our original "electrode micropipette" (Figure 2D). We comprehensively analyzed the endolymph using proteomic approaches and compared the protein profile to our perilymph data (Figures 2E and 3; Table S1). Notably, A2M, OPN, APOD, APOE, and APOJ were enriched in the endolymph (Figure 4; Tables S4 and S5). Moreover, our observations and previous reports indicated that all five proteins were expressed in cells inside the cochlea (Figure 5).

Previously, Salt et al. collected endolymph from the cochleae of guinea pigs using needle-type pipettes made of double-barreled glass capillaries and analyzed the proteins in the fluid using LC-MS.[25,26] In this method, one barrel of the pipette is used to monitor potential, and the other is engaged in sampling. The tip of the double-barreled pipette is likely too large to approach the endolymphatic space of our target animal, i.e., mice, because the size of the cochlea in this species is one-tenth that of guinea pigs. Our "electrode micropipette," which can measure potential with a conductive solvent, was made from a single-barreled capillary (Figure 2D). Therefore, this tool must be an appropriate size for the minuscule cochlea of mice.

Two similarities were detectable in the endolymph profile between our results for mice and data for guinea pigs in previously published literature.[25] The first issue is the protein concentration (mice: 0.50 $\pm$ 0.09 mg/mL, Figure 3A; guinea pigs: 0.38 $\pm$ 0.07 mg/mL). Second, among six proteins identified in guinea-pig endolymph, i.e., α-chymotrypsin, α-antitrypsin, α-HS-glycoprotein, transferrin, APOD, and APOJ, all except α-chymotrypsin were listed in our dataset (Table S1). These observations verified our experimental procedure. From a general standpoint, it should be emphasized that our study, which describes 301 different proteins (Table S1), significantly updates the catalog of endolymph proteins compared to the guinea pig data (six proteins).[25,26] The reason why α-chymotrypsin included in guinea-pig endolymph was undetectable in our list remains unclear, but this inconsistency may mirror differences in analyzed animal species. In addition, our work has dramatically expanded the proteomic catalog of perilymph in genetically unmodified mice. Swan et al. examined the fluid in CBA/CAJ male mice at 3 months of age and identified 50 proteins[39]; in their study, a protein was confirmed when two or more unique peptides were identified. When this criterion was applied to our data from C57BL/6J mice (male, 5 weeks old), 285 proteins were extracted (Table S2). This list contains 74% of the proteins described in CBA/CAJ mice. The reason we could not detect the remainder (13 proteins) may be attributed to differences in animal species or age. Alternatively, because we did not repeat the proteomic analysis, some proteins were missing from the dataset.

Our comprehensive analysis (Figure 2E) revealed that the endolymph contains a diverse array of complement proteins, implying that this fluid serves as a platform for immunity. Additionally, the number and expression levels of proteins that negatively regulate endopeptidase or peptidase activity in the endolymph greatly exceeded those in the perilymph (Figure 3D). Therefore, the endolymph may inhibit proteases and protect endogenous proteins and proteins secreted from the inner ear cells from degradation. Indeed, anti-protease effects are described in α-antitrypsin and α-HS-glycoprotein,[40,41] both of which were present in not only mouse endolymph but also guinea-pig endolymph (Table S1).[25,26]

Particular attention should be paid to the five proteins that were more abundant in the endolymph than in the perilymph (Figure 4). Of these molecules, A2M and APOJ, when tested in cultured cells, can bind to denatured proteins in extracellular fluid; the complexes are likely to be subsequently internalized into cells and subjected to protein digestion.[28] APOE expressed in brain microglia contributes to the regulation of amyloid β (Aβ) aggregation and clearance.[42] In other words, these proteins are likely involved in the removal of "garbage" from the extracellular fluid. Of note, although the endolymph is an extracellular solution, one-third of the proteins that we identified in this lymph using a comprehensive proteomic approach belonged to the intracellular compartments (Figure 2E). This observation suggests that the debris of cochlear cells that have degenerated or been damaged during cellular turnover or aging is released into the endolymph and the denatured or misfolded proteins are caught and cleared up by A2M, APOJ, and APOE. In other words, the endolymph may play a key role in the proteostasis of the cochlea. Additionally, APOD, APOE, and APOJ/CLN are significantly involved in the transport of lipids to cells[43,44]; therefore, endolymph enriched with these proteins may control lipid metabolism in the cochlea more critically than the perilymph. OPN, initially described as an extracellular matrix element in bone tissues,[45,46] occurs in a broad array of immune cell types, including macrophages, neutrophils, dendritic cells, natural killer cells, and lymphocytes.[47,48] Given that OPN is upregulated in response to organ damage or inflammation in bones and skin,[49–51] this molecule likely interacts with different proteins in the immune system in the endolymph and protects the cochlea from foreign substances. Altogether, it is plausible that the endolymph protects the cochlear environment from perturbation with a unique array of proteins, including A2M, OPN, APOD, APOE, and APOJ, in order to control the homeostasis underlying hearing.

It should be emphasized that all five proteins are related to Alzheimer's disease (AD). Of three alleles of the human APOE gene (i.e., ε2, ε3, and ε4), the ε4 allele serves as the highest risk factor for late-onset AD.[52,53] Polymorphisms in the A2M gene are associated with an increased risk of AD.[54] Moreover, A2M protein binds Aβ peptide, prion protein, and β_2-microglobulin, all of which are likely involved in the pathogenesis of AD.[55–57] In patients with AD, APOJ/CLN is upregulated in the hippocampus and cortex,[58] co-localizes with Aβ plaques,[59] and is increased in cerebrospinal fluid.[60] Furthermore, gene polymorphisms are the third risk factor for late-onset AD.[61–63] Additionally, APOJ/CLN can interact with Aβ peptide and promotes its clearance in *in vitro* assays,[64,65] although this effect is controversial in model animals.[66] Similarly, OPN and APOD are elevated in the cerebrospinal fluid of patients with AD.[67,68] As hearing loss is a key promoter of dementia,[12,13] the five proteins enriched in the endolymph may provide a different approach for elucidating the relationship between cochlear dysfunction and cognitive decline.

Limitations of this study

This study has some limitations. The first issue is an inherent drawback of the LC-MS/MS methodology. The MS2 data analysis with "product ion search algorithms" can determine protein sequences precisely. Nevertheless, this strategy is hindered by the issue of sample loss during

the two sequential configurations of MS1 and MS2. As a result, a few proteins which are in fact present in the perilymph and/or endolymph may be missing from our list. Second, because the volume of endolymph sample gathered from multiple mouse cochleae was extremely small, the comprehensive proteomic analysis with LC-MS/MS was carried out only once (Figure 2) and the reproducibility of our data has not been confirmed. Therefore, we cannot rule out the possibility that some proteins detected in the endolymph by the comprehensive analysis (Figure 2E; Table S1) are attributed to contamination of perilymph. Nevertheless, there is no doubt that A2M, OPN, APOD, APOE, and APOJ are more abundant in endolymph than in perilymph because this was confirmed by western blotting (Figure 4B). Finally, the functional significance of the cochlear proteins described in this study has not been examined. These issues need to be addressed in future studies. Nonetheless, our endolymph dataset may contribute to advances in the elucidation of not only the machinery operating the cochlea but also the pathophysiological processes of hearing loss.

RESOURCE AVAILABILITY

Lead contact

Further information and requests for resources and reagents should be directed to and will be fulfilled by the lead contact, Dr. Hiroshi Hibino (hibino@pharma2.med.osaka-u.ac.jp).

Materials availability

This study did not generate new unique reagents.

Data and code availability

- Raw data for the proteomic analysis are available at https://repository.jpostdb.org/entry/JPST003067. Data supporting the findings of this study are available from the corresponding author upon reasonable request.
- This paper does not generate or report any original code.
- Any additional information required to reanalyze the data reported in this paper is available from the lead contact upon request.

ACKNOWLEDGMENTS

We thank all members of the Hibino laboratory for their helpful discussions, Ms. Y. Mizuno for her technical assistance, and Drs. E. Oiki and K. Niwa at the Center for Medical Research and Education, Graduate School of Medicine, Osaka University, for their support in measuring protein content. This study was partly performed under the Collaborative Research Program of the Institute for Protein Research, Osaka University, CR-24-03 (Project Number: 35). This work was supported in part by grants from the Ministry of Education, Culture, Sports, Science and Technology (KAKENHI: 21K06421 and 23H04167), Inamori Foundation, Brain Science Foundation, Narishige Fund, and Takeda Science Foundation to D.I.; and AMED-CREST (Multi-sensing: 24gm1510004 and Mechanobiology: 20gm0810004), Moonshot R&D (JPMJMS2024), and the Ministry of Education, Culture, Sports, Science and Technology (KAKENHI: 24H00798) to H.H. The funders played no role in the study design, data collection and analysis, decision to publish, or manuscript preparation.

AUTHOR CONTRIBUTIONS

D.I., M.F., T.O., and H.H. designed the study. M.F. collected the guinea pig and mouse samples. H.O., T.S., and Y.O. analyzed the endolymph and perilymph samples. M.F., E.W., and K.O. performed immunolabeling assays and RT-PCR. H.H., Y.K., H.I., and M.F. wrote the manuscript. All authors have provided comments on the manuscript.

DECLARATION OF INTERESTS

The authors declare no competing interests.

STAR★METHODS

Detailed methods are provided in the online version of this paper and include the following:

- KEY RESOURCES TABLE
- EXPERIMENTAL MODEL AND STUDY PARTICIPANT DETAILS
  - Animals
  - Cell lines
- METHOD DETAILS
  - Preparation for collection of perilymph and endolymph
  - Sampling of perilymph
  - Sampling of endolymph
  - Determination of protein concentrations of perilymph and endolymph samples
  - Proteomic analysis of endolymph and perilymph
  - LC-MS/MS analyses
  - Western blotting
  - Immunolabeling
  - Quality evaluation of the antibody against A2M
  - Reverse transcription PCR (RT-PCR)
  - Auditory brainstem response (ABR) measurements
- QUANTIFICATION AND STATISTICAL ANALYSIS

SUPPLEMENTAL INFORMATION

Supplemental information can be found online at https://doi.org/10.1016/j.isci.2024.111214.

Received: June 17, 2024
Revised: September 3, 2024
Accepted: October 16, 2024
Published: October 19, 2024

REFERENCES

1. Vassout, P. (1984). Effects of Pure Tone on Endocochlear Potential and Potassium Ion Concentration in the Guinea Pig Cochlea. Acta Otolaryngol. *98*, 199–203. https://doi.org/10.3109/00016488409107555.
2. Anniko, M., and Wróblewski, R. (1986). Ionic Environment of Cochlear Hair Cells. Hear. Res. *22*, 279–293. https://doi.org/10.1016/0378-5955(86)90104-8.
3. Yamasaki, M., Komune, S., Shimozono, M., Matsuda, K., and Haruta, A. (2000). Development of Monovalent Ions in the Endolymph in Mouse Cochlea. ORL. J. Otorhinolaryngol. Relat. Spec. *62*, 241–246. https://doi.org/10.1159/000027753.
4. Hibino, H., Nin, F., Tsuzuki, C., and Kurachi, Y. (2010). How Is the Highly Positive Endocochlear Potential Formed? The Specific Architecture of the Stria Vascularis and the Roles of the Ion-Transport Apparatus. Pflugers Arch. *459*, 521–533. https://doi.org/10.1007/s00424-009-0754-z.
5. Nin, F., Hibino, H., Doi, K., Suzuki, T., Hisa, Y., and Kurachi, Y. (2008). The Endocochlear Potential Depends on Two K+ Diffusion Potentials and an Electrical Barrier in the Stria Vascularis of the Inner Ear. Proc. Natl. Acad. Sci. USA *105*, 1751–1756. https://doi.org/10.1073/pnas.0711463105.
6. Rybak, L.P., Whitworth, C., and Scott, V. (1992). Development of Endocochlear Potential and Compound Action Potential in the Rat. Hear. Res. *59*, 189–194. https://doi.org/10.1016/0378-5955(92)90115-4.
7. Tasaki, I., and Spyropoulos, C.S. (1959). Stria Vascularis as Source of Endocochlear Potential. J. Neurophysiol. *22*, 149–155. https://doi.org/10.1152/jn.1959.22.2.149.
8. Sato, M.P., Higuchi, T., Nin, F., Ogata, G., Sawamura, S., Yoshida, T., Ota, T., Hori, K., Komune, S., Uetsuka, S., et al. (2017). Hearing Loss Controlled by Optogenetic Stimulation of Nonexcitable Nonglial Cells in the Cochlea of the Inner Ear. Front. Mol. Neurosci. *10*, 300. https://doi.org/10.3389/fnmol.2017.00300.
9. Nin, F., Yoshida, T., Sawamura, S., Ogata, G., Ota, T., Higuchi, T., Murakami, S., Doi, K., Kurachi, Y., and Hibino, H. (2016). The Unique Electrical Properties in an Extracellular Fluid of the Mammalian Cochlea; Their Functional Roles, Homeostatic Processes, and Pathological Significance. Pflugers Arch. *468*, 1637–1649. https://doi.org/10.1007/s00424-016-1871-0.
10. Hibino, H., and Kurachi, Y. (2006). Molecular and Physiological Bases of the K+ Circulation in the Mammalian Inner Ear. Physiology *21*, 336–345. https://doi.org/10.1152/physiol.00023.2006.
11. Kikuchi, T., Kimura, R.S., Paul, D.L., Takasaka, T., and Adams, J.C. (2000). Gap Junction Systems in the Mammalian Cochlea. Brain Res. Brain Res. Rev. *32*, 163–166. https://doi.org/10.1016/s0165-0173(99)00076-4.
12. Livingston, G., Sommerlad, A., Orgeta, V., Costafreda, S.G., Huntley, J., Ames, D., Ballard, C., Banerjee, S., Burns, A., Cohen-Mansfield, J., et al. (2017). Dementia Prevention, Intervention, and Care. Lancet *390*, 2673–2734. https://doi.org/10.1016/S0140-6736(17)31363-6.
13. Livingston, G., Huntley, J., Sommerlad, A., Ames, D., Ballard, C., Banerjee, S., Brayne, C., Burns, A., Cohen-Mansfield, J., Cooper, C., et al. (2020). Dementia Prevention, Intervention, and Care: 2020 Report of the Lancet Commission. Lancet *396*, 413–446. https://doi.org/10.1016/S0140-6736(20)30367-6.
14. Yamasoba, T., Lin, F.R., Someya, S., Kashio, A., Sakamoto, T., and Kondo, K. (2013). Current Concepts in Age-Related Hearing Loss: Epidemiology and Mechanistic Pathways. Hear. Res. *303*, 30–38. https://doi.org/10.1016/j.heares.2013.01.021.
15. Lanvers-Kaminsky, C., Zehnhoff-Dinnesen, A.A., Parfitt, R., and Ciarimboli, G. (2017). Drug-Induced Ototoxicity: Mechanisms, Pharmacogenetics, and Protective Strategies. Clin. Pharmacol. Ther. *101*, 491–500. https://doi.org/10.1002/cpt.603.
16. Oishi, N., and Schacht, J. (2011). Emerging Treatments for Noise-Induced Hearing Loss. Expet Opin. Emerg. Drugs *16*, 235–245. https://doi.org/10.1517/14728214.2011.552427.
17. Cunningham, L.L., and Tucci, D.L. (2017). Hearing Loss in Adults. N. Engl. J. Med. *377*, 2465–2473. https://doi.org/10.1056/NEJMra1616601.
18. Korver, A.M.H., Smith, R.J.H., Van Camp, G., Schleiss, M.R., Bitner-Glindzicz, M.A.K., Lustig, L.R., Usami, S.I., and Boudewyns, A.N. (2017). Congenital Hearing Loss. Nat. Rev. Dis. Prim. *3*, 16094. https://doi.org/10.1038/nrdp.2016.94.
19. Abe, S., Usami, S., Shinkawa, H., Kelley, P.M., and Kimberling, W.J. (2000). Prevalent Connexin 26 Gene (GJB2) Mutations in Japanese. J. Med. Genet. *37*, 41–43. https://doi.org/10.1136/jmg.37.1.41.
20. Sloan-Heggen, C.M., Bierer, A.O., Shearer, A.E., Kolbe, D.L., Nishimura, C.J., Frees, K.L., Ephraim, S.S., Shibata, S.B., Booth, K.T., Campbell, C.A., et al. (2016). Comprehensive Genetic Testing in the Clinical Evaluation of 1119 Patients With Hearing Loss. Hum. Genet. *135*, 441–450. https://doi.org/10.1007/s00439-016-1648-8.
21. Ohlemiller, K.K. (2006). Contributions of Mouse Models to Understanding of Age- and Noise-Related Hearing Loss. Brain Res. *1091*, 89–102. https://doi.org/10.1016/j.brainres.2006.03.017.
22. Fernandez, K., Wafa, T., Fitzgerald, T.S., and Cunningham, L.L. (2019). An Optimized, Clinically Relevant Mouse Model of Cisplatin-Induced Ototoxicity. Hear. Res. *375*, 66–74. https://doi.org/10.1016/j.heares.2019.02.006.
23. Thorne, M., Salt, A.N., DeMott, J.E., Henson, M.M., Henson, O.W., Jr., and Gewalt, S.L. (1999). Cochlear Fluid Space Dimensions for Six Species Derived From Reconstructions of Three-Dimensional Magnetic Resonance Images. Laryngoscope *109*, 1661–1668. https://doi.org/10.1097/00005537-199910000-00021.
24. Hirose, K., Hartsock, J.J., Johnson, S., Santi, P., and Salt, A.N. (2014). Systemic Lipopolysaccharide Compromises the Blood-Labyrinth Barrier and Increases Entry of Serum Fluorescein Into the Perilymph. J. Assoc. Res. Otolaryngol. *15*, 707–719. https://doi.org/10.1007/s10162-014-0476-6.
25. Thalmann, I., Hughes, I., Tong, B.D., Ornitz, D.M., and Thalmann, R. (2006). Microscale Analysis of Proteins in Inner Ear Tissues and Fluids With Emphasis on Endolymphatic Sac, Otoconia, and Organ of Corti. Electrophoresis *27*, 1598–1608. https://doi.org/10.1002/elps.200500768.
26. Thalmann, I., Comegys, T.H., Liu, S.Z., Ito, Z., and Thalmann, R. (1992). Protein Profiles of Perilymph and Endolymph of the Guinea Pig. Hear. Res. *63*, 37–42. https://doi.org/10.1016/0378-5955(92)90071-t.
27. Laforge, F.O., Carpino, J., Rotenberg, S.A., and Mirkin, M.V. (2007). Electrochemical Attosyringe. Proc. Natl. Acad. Sci. USA *104*, 11895–11900. https://doi.org/10.1073/pnas.0705102104.
28. Tomihari, A., Kiyota, M., Matsuura, A., and Itakura, E. (2023). Alpha 2-Macroglobulin Acts as a Clearance Factor in the Lysosomal Degradation of Extracellular Misfolded Proteins. Sci. Rep. *13*, 4680. https://doi.org/10.1038/s41598-023-31104-x.
29. Lauer, D., Reichenbach, A., and Birkenmeier, G. (2001). α 2-Macroglobulin-Mediated Degradation of Amyloid β1–42: A Mechanism to Enhance Amyloid β Catabolism. Exp. Neurol. *167*, 385–392. https://doi.org/10.1006/exnr.2000.7569.
30. Konings, S.C., Nyberg, E., Martinsson, I., Torres-Garcia, L., Klementieva, O., Guimas Almeida, C., and Gouras, G.K. (2023). Apolipoprotein E Intersects With Amyloid-β Within Neurons. Life Sci. Alliance *6*, e202201887. https://doi.org/10.26508/lsa.202201887.
31. Yerbury, J.J., Poon, S., Meehan, S., Thompson, B., Kumita, J.R., Dobson, C.M., and Wilson, M.R. (2007). The Extracellular Chaperone Clusterin Influences Amyloid Formation and Toxicity by Interacting With Prefibrillar Structures. FASEB J. *21*, 2312–2322. https://doi.org/10.1096/fj.06-7986com.
32. Wyatt, A.R., Yerbury, J.J., Berghofer, P., Greguric, I., Katsifis, A., Dobson, C.M., and Wilson, M.R. (2011). Clusterin Facilitates In Vivo Clearance of Extracellular Misfolded

Proteins. Cell. Mol. Life Sci. *68*, 3919–3931. https://doi.org/10.1007/s00018-011-0684-8.
33. Zheng, R., Zhang, Y., Zhang, K., Yuan, Y., Jia, S., and Liu, J. (2022). The Complement System, Aging, and Aging-Related Diseases. Int. J. Mol. Sci. *23*, 8689. https://doi.org/10.3390/ijms23158689.
34. Hildebrand, M.S., de Silva, M.G., Klockars, T., Solares, C.A., Hirose, K., Smith, J.D., Patel, S.C., and Dahl, H.H.M. (2005). Expression of the Carrier Protein Apolipoprotein D in the Mouse Inner Ear. Hear. Res. *200*, 102–114. https://doi.org/10.1016/j.heares.2004.08.018.
35. Sakagami, M. (2000). Role of Osteopontin in the Rodent Inner Ear as Revealed by In Situ Hybridization. Med. Electron. Microsc. *33*, 3–10. https://doi.org/10.1007/s007950000001.
36. Zhao, X., Henderson, H.J., Wang, T., Liu, B., and Li, Y. (2021). Deletion of Clusterin Protects Cochlear Hair Cells Against Hair Cell Aging and Ototoxicity. Neural Plast. *2021*, 9979157. https://doi.org/10.1155/2021/9979157.
37. Liu, H., Chen, L., Giffen, K.P., Stringham, S.T., Li, Y., Judge, P.D., Beisel, K.W., and He, D.Z.Z. (2018). Cell-Specific Transcriptome Analysis Shows That Adult Pillar and Deiters' Cells Express Genes Encoding Machinery for Specializations of Cochlear Hair Cells. Front. Mol. Neurosci. *11*, 356. https://doi.org/10.3389/fnmol.2018.00356.
38. Yue, F., Cheng, Y., Breschi, A., Vierstra, J., Wu, W., Ryba, T., Sandstrom, R., Ma, Z., Davis, C., Pope, B.D., et al. (2014). A Comparative Encyclopedia of DNA Elements in the Mouse Genome. Nature *515*, 355–364. https://doi.org/10.1038/nature13992.
39. Swan, E.E.L., Peppi, M., Chen, Z., Green, K.M., Evans, J.E., McKenna, M.J., Mescher, M.J., Kujawa, S.G., and Sewell, W.F. (2009). Proteomics Analysis of Perilymph and Cerebrospinal Fluid in Mouse. Laryngoscope *119*, 953–958. https://doi.org/10.1002/lary.20209.
40. Gettins, P.G.W. (2002). Serpin Structure, Mechanism, and Function. Chem. Rev. *102*, 4751–4804. https://doi.org/10.1021/cr010170+.
41. Hedrich, J., Lottaz, D., Meyer, K., Yiallouros, I., Jahnen-Dechent, W., Stöcker, W., and Becker-Pauly, C. (2010). Fetuin-A and Cystatin C Are Endogenous Inhibitors of Human Meprin Metalloproteases. Biochemistry *49*, 8599–8607. https://doi.org/10.1021/bi1004238.
42. Wisniewski, T., and Drummond, E. (2020). APOE-Amyloid Interaction: Therapeutic Targets. Neurobiol. Dis. *138*, 104784. https://doi.org/10.1016/j.nbd.2020.104784.
43. Dominiczak, M.H., and Caslake, M.J. (2011). Apolipoproteins: Metabolic Role and Clinical Biochemistry Applications. Ann. Clin. Biochem. *48*, 498–515. https://doi.org/10.1258/acb.2011.011111.
44. Heo, J.Y., Kim, J.E., Dan, Y., Kim, Y.W., Kim, J.Y., Cho, K.H., Bae, Y.K., Im, S.S., Liu, K.H., Song, I.H., et al. (2018). Clusterin Deficiency Induces Lipid Accumulation and Tissue Damage in Kidney. J. Endocrinol. *237*, 175–191. https://doi.org/10.1530/JOE-17-0453.
45. Butler, W.T. (1989). The Nature and Significance of Osteopontin. Connect. Tissue Res. *23*, 123–136. https://doi.org/10.3109/03008208909002412.
46. Icer, M.A., and Gezmen-Karadag, M. (2018). The Multiple Functions and Mechanisms of Osteopontin. Clin. Biochem. *59*, 17–24. https://doi.org/10.1016/j.clinbiochem.2018.07.003.
47. Wang, K.X., and Denhardt, D.T. (2008). Osteopontin: Role in Immune Regulation and Stress Responses. Cytokine Growth Factor Rev. *19*, 333–345. https://doi.org/10.1016/j.cytogfr.2008.08.001.
48. Lund, S.A., Giachelli, C.M., and Scatena, M. (2009). The Role of Osteopontin in Inflammatory Processes. J. Cell Commun. Signal. *3*, 311–322. https://doi.org/10.1007/s12079-009-0068-0.
49. Si, J., Wang, C., Zhang, D., Wang, B., and Zhou, Y. (2020). Osteopontin in Bone Metabolism and Bone Diseases. Med. Sci. Monit. *26*, e919159. https://doi.org/10.12659/MSM.919159.
50. Buommino, E., Tufano, M.A., Balato, N., Canozo, N., Donnarumma, M., Gallo, L., Balato, A., and Ayala, F. (2009). Osteopontin: a New Emerging Role in Psoriasis. Arch. Dermatol. Res. *301*, 397–404. https://doi.org/10.1007/s00403-009-0939-5.
51. Lamort, A.S., Giopanou, I., Psallidas, I., and Stathopoulos, G.T. (2019). Osteopontin as a Link Between Inflammation and Cancer: the Thorax in the Spotlight. Cells *8*, 815. https://doi.org/10.3390/cells8080815.
52. Serrano-Pozo, A., Das, S., and Hyman, B.T. (2021). APOE and Alzheimer's Disease: Advances in Genetics, Pathophysiology, and Therapeutic Approaches. Lancet Neurol. *20*, 68–80. https://doi.org/10.1016/S1474-4422(20)30412-9.
53. Corder, E.H., Saunders, A.M., Strittmatter, W.J., Schmechel, D.E., Gaskell, P.C., Small, G.W., Roses, A.D., Haines, J.L., and Pericak-Vance, M.A. (1993). Gene Dose of Apolipoprotein E Type 4 Allele and the Risk of Alzheimer's Disease in Late Onset Families. Science *261*, 921–923. https://doi.org/10.1126/science.8346443.
54. Zill, P., Bürger, K., Behrens, S., Hampel, H., Padberg, F., Boetsch, T., Möller, H.J., Ackenheil, M., and Bondy, B. (2000). Polymorphisms in the Alpha-2 Macroglobulin Gene in Psychogeriatric Patients. Neurosci. Lett. *294*, 69–72. https://doi.org/10.1016/s0304-3940(00)01518-4.
55. Wyatt, A.R., Constantinescu, P., Ecroyd, H., Dobson, C.M., Wilson, M.R., Kumita, J.R., and Yerbury, J.J. (2013). Protease-Activated Alpha-2-Macroglobulin Can Inhibit Amyloid Formation via Two Distinct Mechanisms. FEBS Lett. *587*, 398–403. https://doi.org/10.1016/j.febslet.2013.01.020.
56. Mantuano, E., Azmoon, P., Banki, M.A., Gunner, C.B., and Gonias, S.L. (2022). The LRP1/CD91 Ligands, Tissue-Type Plasminogen Activator, α(2)-Macroglobulin, and Soluble Cellular Prion Protein Have Distinct co-Receptor Requirements for Activation of Cell-Signaling. Sci. Rep. *12*, 17594. https://doi.org/10.1038/s41598-022-22498-1.
57. Argilés, A., Mourad, G., Gouin-Charnet, A., and Schmitt-Bernard, C.F. (2000). Antiproteases and Cells in the Pathogenesis of Beta(2)-Microglobulin Amyloidosis: Role of Alpha(2)-Macroglobulin and Macrophages. Nephron *86*, 1–11. https://doi.org/10.1159/000045707.
58. Lidström, A.M., Bogdanovic, N., Hesse, C., Volkman, I., Davidsson, P., and Blennow, K. (1998). Clusterin (Apolipoprotein J) Protein Levels Are Increased in Hippocampus and in Frontal Cortex in Alzheimer's Disease. Exp. Neurol. *154*, 511–521. https://doi.org/10.1006/exnr.1998.6892.
59. Martin-Rehrmann, M.D., Hoe, H.S., Capuani, E.M., and Rebeck, G.W. (2005). Association of Apolipoprotein J-Positive Beta-Amyloid Plaques With Dystrophic Neurites in Alzheimer's Disease Brain. Neurotox. Res. *7*, 231–242. https://doi.org/10.1007/BF03036452.
60. Wang, H., Ma, L.Z., Sheng, Z.H., Liu, J.Y., Yuan, W.Y., Guo, F., Zhang, W., and Tan, L. (2023). Association Between Cerebrospinal Fluid Clusterin and Biomarkers of Alzheimer's Disease Pathology in Mild Cognitive Impairment: a Longitudinal Cohort Study. Front. Aging Neurosci. *15*, 1256389. https://doi.org/10.3389/fnagi.2023.1256389.
61. Harold, D., Abraham, R., Hollingworth, P., Sims, R., Gerrish, A., Hamshere, M.L., Pahwa, J.S., Moskvina, V., Dowzell, K., Williams, A., et al. (2009). Genome-Wide Association Study Identifies Variants at CLU and PICALM Associated With Alzheimer's Disease. Nat. Genet. *41*, 1088–1093. https://doi.org/10.1038/ng.440.
62. Foster, E.M., Dangla-Valls, A., Lovestone, S., Ribe, E.M., and Buckley, N.J. (2019). Clusterin in Alzheimer's Disease: Mechanisms, Genetics, and Lessons From Other Pathologies. Front. Neurosci. *13*, 164. https://doi.org/10.3389/fnins.2019.00164.
63. Lambert, J.C., Heath, S., Even, G., Campion, D., Sleegers, K., Hiltunen, M., Combarros, O., Zelenika, D., Bullido, M.J., Tavernier, B., et al. (2009). Genome-Wide Association Study Identifies Variants at CLU and CR1 Associated With Alzheimer's Disease. Nat. Genet. *41*, 1094–1099. https://doi.org/10.1038/ng.439.
64. Yeh, F.L., Wang, Y., Tom, I., Gonzalez, L.C., and Sheng, M. (2016). TREM2 Binds to Apolipoproteins, Including APOE and CLU/APOJ, and Thereby Facilitates Uptake of Amyloid-Beta by Microglia. Neuron *91*, 328–340. https://doi.org/10.1016/j.neuron.2016.06.015.
65. Merino-Zamorano, C., Fernández-de Retana, S., Montañola, A., Batlle, A., Saint-Pol, J., Mysiorek, C., Gosselet, F., Montaner, J., and Hernández-Guillamon, M. (2016). Modulation of Amyloid-β1-40 Transport by ApoA1 and ApoJ Across an In Vitro Model of the Blood-Brain Barrier. J. Alzheimers Dis. *53*, 677–691. https://doi.org/10.3233/JAD-150976.
66. DeMattos, R.B., O'dell, M.A., Parsadanian, M., Taylor, J.W., Harmony, J.A.K., Bales, K.R., Paul, S.M., Aronow, B.J., and Holtzman, D.M. (2002). Clusterin Promotes Amyloid Plaque Formation and Is Critical for Neuritic Toxicity in a Mouse Model of Alzheimer's Disease. Proc. Natl. Acad. Sci. USA *99*, 10843–10848. https://doi.org/10.1073/pnas.162228299.
67. Sun, Y., Yin, X.S., Guo, H., Han, R.K., He, R.D., and Chi, L.J. (2013). Elevated Osteopontin Levels in Mild Cognitive Impairment and Alzheimer's Disease. Mediators Inflamm. *2013*, 615745. https://doi.org/10.1155/2013/615745.
68. Kalman, J., McConathy, W., Araoz, C., Kasa, P., and Lacko, A.G. (2000). Apolipoprotein D in the Aging Brain and in Alzheimer's Dementia. Neurol. Res. *22*, 330–336. https://doi.org/10.1080/01616412.2000.11740678.
69. Kilkenny, C., Browne, W.J., Cuthill, I.C., Emerson, M., and Altman, D.G. (2010). Improving Bioscience Research Reporting: the ARRIVE Guidelines for Reporting Animal Research. PLoS Biol. *8*, e1000412. https://doi.org/10.1371/journal.pbio.1000412.

70. Poklonnov, V., Martynov, L., Astafiev, A., and Zaitsev, N. (2022). Voltammetric Studies of Glutathione Transfer Across Arrays of Liquid-Liquid Microinterfaces for Sensing Applications. Amino Acids *54*, 911–922. https://doi.org/10.1007/s00726-022-03166-0.
71. Yu, H., Yzeiri, I., Hou, B., Chen, C.H., Bu, W., Vanysek, P., Chen, Y.S., Lin, B., Král, P., and Schlossman, M.L. (2015). Electric Field Effect on Phospholipid Monolayers at an Aqueous-Organic Liquid-Liquid Interface. J. Phys. Chem. B *119*, 9319–9334. https://doi.org/10.1021/jp5098525.
72. Hibino, H., Horio, Y., Inanobe, A., Doi, K., Ito, M., Yamada, M., Gotow, T., Uchiyama, Y., Kawamura, M., Kubo, T., and Kurachi, Y. (1997). An ATP-Dependent Inwardly Rectifying Potassium Channel, KAB-2 (Kir4. 1), in Cochlear Stria Vascularis of Inner Ear: Its Specific Subcellular Localization and Correlation with the Formation of Endocochlear Potential. J. Neurosci. *17*, 4711–4721. https://doi.org/10.1523/JNEUROSCI.17-12-04711.1997.
73. Salt, A.N., Hale, S.A., and Plonkte, S.K.R. (2006). Perilymph Sampling From the Cochlear Apex: a Reliable Method to Obtain Higher Purity Perilymph Samples From Scala Tympani. J. Neurosci. Methods *153*, 121–129. https://doi.org/10.1016/j.jneumeth.2005.10.008.
74. Deng, Y., Chen, D., Gao, F., Lv, H., Zhang, G., Sun, X., Liu, L., Mo, D., Ma, N., Song, L., et al. (2020). Silencing of Long Non-coding RNA GAS5 Suppresses Neuron Cell Apoptosis and Nerve Injury in Ischemic Stroke Through Inhibiting DNMT3B-Dependent MAP4K4 Methylation. Transl. Stroke Res. *11*, 950–966. https://doi.org/10.1007/s12975-019-00770-3.
75. Sekiguchi, N., Kubo, C., Takahashi, A., Muraoka, K., Takeiri, A., Ito, S., Yano, M., Mimoto, F., Maeda, A., Iwayanagi, Y., et al. (2018). MHC-Associated Peptide Proteomics Enabling Highly Sensitive Detection of Immunogenic Sequences for the Development of Therapeutic Antibodies With Low Immunogenicity. mAbs *10*, 1168–1181. https://doi.org/10.1080/19420862.2018.1518888.
76. Murai, M., and Miyoshi, H. (2019). Photoaffinity Labeling of Respiratory Complex I in Bovine Heart Submitochondrial Particles by Photoreactive [(125)I] Amilorides. Bio. Protoc. *9*, e3349. https://doi.org/10.21769/BioProtoc.3349.
77. Tsugawa, H., Kabe, Y., Kanai, A., Sugiura, Y., Hida, S., Taniguchi, S., Takahashi, T., Matsui, H., Yasukawa, Z., Itou, H., et al. (2020). Short-Chain Fatty Acids Bind to Apoptosis-Associated Speck-Like Protein to Activate Inflammasome Complex to Prevent Salmonella Infection. PLoS Biol. *18*, e3000813. https://doi.org/10.1371/journal.pbio.3000813.
78. Granvogl, B., Plöscher, M., and Eichacker, L.A. (2007). Sample Preparation by in-Gel Digestion for Mass Spectrometry-Based Proteomics. Anal. Bioanal. Chem. *389*, 991–1002. https://doi.org/10.1007/s00216-007-1451-4.
79. Okanishi, H., Ohgaki, R., Okuda, S., Endou, H., and Kanai, Y. (2021). Proteomics and Phosphoproteomics Reveal Key Regulators Associated With Cytostatic Effect of Amino Acid Transporter LAT1 Inhibitor. Cancer Sci. *112*, 871–883. https://doi.org/10.1111/cas.14756.
80. Khunweeraphong, N., Nagamori, S., Wiriyasermkul, P., Nishinaka, Y., Wongthai, P., Ohgaki, R., Tanaka, H., Tominaga, H., Sakurai, H., and Kanai, Y. (2012). Establishment of Stable Cell Lines with High Expression of Heterodimers of Human 4F2hc and Human Amino Acid Transporter LAT1 or LAT2 and Delineation of Their Differential Interaction with α-Alkyl Moieties. J. Pharmacol. Sci. *119*, 368–380. https://doi.org/10.1254/jphs.12124fp.
81. Cusack, J.C., Jr., Liu, R., Houston, M., Abendroth, K., Elliott, P.J., Adams, J., and Baldwin, A.S., Jr. (2001). Enhanced Chemosensitivity to CPT-11 with Proteasome Inhibitor PS-341: Implications for Systemic Nuclear Factor-kappaB Inhibition. Cancer Res. *61*, 3535–3540.
82. Hibino, H., Higashi-Shingai, K., Fujita, A., Iwai, K., Ishii, M., and Kurachi, Y. (2004). Expression of an Inwardly Rectifying K+ Channel, Kir5.1, in Specific Types of Fibrocytes in the Cochlear Lateral Wall Suggests Its Functional Importance in the Establishment of Endocochlear Potential. Eur. J. Neurosci. *19*, 76–84. https://doi.org/10.1111/j.1460-9568.2004.03092.x.
83. Ishii, M., Fujita, A., Iwai, K., Kusaka, S., Higashi, K., Inanobe, A., Hibino, H., and Kurachi, Y. (2003). Differential Expression and Distribution of Kir5.1 and Kir4.1 Inwardly Rectifying K+ Channels in Retina. Am. J. Physiol. Cell Physiol. *285*, C260–C267. https://doi.org/10.1152/ajpcell.00560.2002.

STAR★METHODS

KEY RESOURCES TABLE

REAGENT or RESOURCE	SOURCE	IDENTIFIER
Antibodies		
A2M Recombinant Rabbit Monoclonal Antibody	Invitrogen	MA5-38211; RRID: AB_2898128
Mouse Osteopontin/OPN Antibody	biotechne	AF808; RRID: AB_2194992
Apolipoprotein E Antibody	Sigma-Aldrich	AB947; RRID: AB_2258475
Apolipoprotein D Polyclonal Antibody	Invitrogen	PA5-27386; RRID: AB_2544862
Mouse Clusterin Antibody	biotechne	AF2747; RRID: AB_2083314
Peroxidase AffiniPure™ Goat Anti-Rabbit IgG (H + L)	Jackson ImmunoResearch Laboratories	RRID: AB_2307391
Anti-Albumin antibody	abcam	ab207327; RRID: AB_2755031
Beta Actin Monoclonal antibody	proteintech	Cat No. 66009-1-Ig; RRID: AB_2687938
Anti-alpha 2 Macroglobulin antibody	Abcam	Ab58703; RRID: AB_879541
Goat anti-Rabbit IgG (H + L) Cross-Adsorbed Secondary Antibody, Alexa Fluor™ 568	ThermoFisherScientific	Cat # A-11011; RRID: AB_143157
c-MYC Polyclonal antibody	proteintech	Cat No. 10828-1-AP; RRID: AB_2148585
Goat Anti-Rabbit IgG H&L (Alexa Fluor® 488)	abcam	ab150077; RRID: AB_2630356
Chemicals, peptides, and recombinant proteins		
DAPI and Hoechst Nucleic Acid Stains	ThermoFisherScientific	Cat # 62248
Skim Milk Powder	Wako	JAN4987481423558
Polyoxyethylene(20) Sorbitan Monolaurate	Wako	JAN4987481429147
Amersham ECL Prime Western Blotting Detection Reagent	Cytiva	RPN2232
optimum cutting temperature compound	Sakura Finetechnology	45833
PBS	Wako	JAN4548995063342
Blocking Reagent	Roche	10057177103
STANDARD GLASS CAPILLARIES	WPI	1B150F-4
Tetradodecylammoniumtetrakis(4-chlorophenyl)borate	Sigma-Aldrich	87255
1,2-dichloroethane	Wako	JAN4987481432598
SuperSep (TM) Ace, 5–20%, 17well	Wako	JAN4987481477759
Critical commercial assays		
TaKaRa Bradford Protein Assay Kit	TaKaRa	T9310A
Silver Stain 2 Kit wako	Wako	JAN4987481359772
PureLink™ RNA Mini Kit	ThermoFisherScientific	12183018A
PrimeScript™ IV 1st strand cDNA Synthesis Mix	Takara bio	6215A
Deposited data		
Raw data for the proteomic analysis	N/A	https://repository.jpostdb.org/entry/JPST003067
Experimental models: Cell lines		
Human: HEK293T cells	ATCC	RRID:CVCL_B0XW
Experimental models: Organisms/strains		
Mice: C57BL/6J JmsSlc	SLC	http://www.jslc.co.jp/animals/mouse.php
Guinea pigs: Hartley	SLC	http://www.jslc.co.jp/english/animals/other.php

(*Continued on next page*)

Continued

REAGENT or RESOURCE	SOURCE	IDENTIFIER
Recombinant DNA		
pDNA(VB231220-1997ybb)	This paper	N/A
Software and algorithms		
Fiji	Fiji	https://fiji.sc RRID: SCR_002285
FD223a	WPI	chrome-extension://efaidnbmnnnibpcajpcglclefindmkaj/ https://www.wpiinc.com/media/wysiwyg/pdf/DS/FD223a.pdf
BioSigRZ	Tucker-Davis Technologies	https://www.tdt.com/component/ biosigrz-abr-dpoae-software/RRID: SCR_014820
LSM 880 with an Airyscan confocal microscope	Zeiss	https://imaging.wehi.edu.au/our-instruments/zeiss-lsm-880
ChemiDoc XRS	Bio-Rad	1708265J1NPC
Q-Exactive Orbitrap mass spectrometer	ThermoFisherScientific	BRE725600
C1000 Touch Thermal Cycler	BIO-RAD	1851148JA RRID: SCR_019690
DAVID	National Institute of Hearth	https://david.ncifcrf.gov/summary.jsp RRID: SCR_001881
Microsoft Excel		https://www.microsoft.com/en-gb/RRID:SCR_016137

EXPERIMENTAL MODEL AND STUDY PARTICIPANT DETAILS

Animals

C57/BL6J (SLC Inc., Hamamatsu, Japan) male mice at 5 weeks of age and male Hartley albino guinea pigs (SLC) at 3 weeks of age were used in this study. All animals were housed at the animal facility of Osaka University Graduate School of Medicine and kept at 23 ± 1.5°C in a 12-h light/12-h dark cycle. Food and water were provided *ad libitum*. The experiments were performed during the light period of the cycle. Efforts were taken to reduce the suffering of experimental animals to the maximum extent possible. The animals were randomly assigned to each experiment. No blinding was conducted.

Initially, each mouse was anesthetized by an intraperitoneal injection of a mixture of medetomidine hydrochloride (0.75 mg/kg bw; Kyoritsu Seiyaku, Tokyo, Japan), midazolam (4 mg/kg bw; Sando, Tokyo, Japan), and butorfal tartrate (5 mg/kg bw; Meiji Seika Farma, Tokyo, Japan). Guinea pigs were anesthetized by intraperitoneal injection of a mixture of xylazine hydrochloride (40 mg/kg bw; Fujita, Tokyo, Japan) and ketamine hydrochloride (5 mg/kg bw; Daiichisankyo, Tokyo, Japan).

To evaluate the depth of anesthesia, toe pinch, corneal reflexes, and respiratory rate were examined in accordance with the guidelines. When anesthesia was insufficient, a mixture of medetomidine hydrochloride (0.375 mg/kg bw), midazolam (2 mg/kg bw), and butorfal tartrate (2.5 mg/kg bw) and a mixture of xylazine hydrochloride (40 mg/kg bw) and ketamine hydrochloride (5 mg/kg bw) were administered. After deep anesthesia was confirmed, the mice and guinea pigs were subjected to each experiment. During the experiment, animals were maintained with spontaneous respiration and the body temperature was kept near 37°C with a heating pad (Natsume Seisakusho, Tokyo, Japan). After the experiment, the animals were euthanized with an overdose of anesthetic.

All experimental protocols involving animals were approved by the Animal Care and Use Committee of Osaka University Graduate School of Medicine (Reference Number: 04-063-002). The experiments were performed under the supervision of the committee and in accordance with the Guidelines for Animal Experiments of Osaka University and the Japanese Animal Protection and Management Law. All animal handling and reporting procedures complied with ARRIVE guidelines.[69]

Cell lines

HEK293T cells (RRID:CVCL_B0XW) was obtained from American Type Culture Collection (ATCC, Manassas, VA, USA). The cells were presumably authenticated by ATCC and were not further authenticated in this study. The cell lines, which routinely tested negative for mycoplasma contamination, were maintained in DMEM supplemented with 10% (v/v) fetal bovine serum (FBS) and 100 μg/mL ampicillin in an atmosphere of 95% air and 5% CO2 at 37°C.

METHOD DETAILS

Preparation for collection of perilymph and endolymph

For each collection trial, a single-barreled glass capillary was pulled to fabricate a needle-type pipette, and then the tip was beveled to a diameter of ~10 μm and ~4 μm for endolymph and perilymph sampling, respectively. The pipette used for endolymph sampling was then filled with 10 mM tetradodecylammonium tetrakis 4-chlorophenyl borate (TDATPBCL) dissolved in 1,2-dichloroethane (DCE) solution (TDATPBCL; Merck KGaA, Darmstadt, Germany) (DCE; Fujifilm, Tokyo, Japan). The long carbon chain in TDATPBCL is hydrophobic and the anions and cations in DCE solution can conduct electricity[70,71] (Figure 2A). The barrel was connected via an Ag/AgTPBCl electrode to

an electrometer. This needle-type tool served not only as an electrode for measuring potential but also as a pipette for aspirating hydrophilic liquids; therefore, it is termed an 'electrode micropipette.'

Sampling of perilymph

A total of 8 mice (16 cochleae) were used for perilymph analysis. Each mouse was deeply anesthetized as described above and mounted on a head holder. First, the left cochlea was exposed using a ventrolateral approach.[72] Perilymph was sampled according to the method described by Salt et al.[73] We accessed the apex of the cochlea to minimize contamination of the cerebrospinal fluid (CSF) connected to the perilymph in the basal turn through a narrow tubule.[73] A small fenestra was made with a sharp needle on top of the apical portion of the bony wall where moisture was thoroughly removed in advance using a cotton swab. A glass pipette was inserted through the fenestra into the scala tympani using a micromanipulator (MP-285; Sutter Instrument Co., Novato, CA, USA). When the pipette reached this space, perilymph automatically flowed into the pipette. From each cochlea, an aliquot of 0.5–0.9 μL was collected. Perilymph samples were obtained from both cochleae of each animal. For each series of biochemical assay, aliquots from 2 to 3 cochleae were gathered in a Protein LoBind tube (0.5 mL; Eppendorf, Hamburg, Germany) (final sample volume: ∼1.5 μL for proteomic analysis and ∼1 μL for western blotting, respectively). A total of 0.4 μL of the homogenized sample was used for protein concentration measurement, whereas volumes corresponding to 0.9 μg protein (∼1 μL) and 0.6 μg protein (∼0.6 μL) were subjected to comprehensive proteomics analysis and western blotting, respectively.

Sampling of endolymph

A total of 171 mice (342 cochleae) were subjected to *in vivo* experiments to collect endolymph. Animal preparations and resulting data were excluded if any of the following two conditions were met: When a middle ear deformity or effusion was observed during surgery, the experiment was no longer performed (12 cochleae). Second, we did not proceed with sampling of the endolymph in mice in which the endolymph potential measured by the electrode micropipette did not exceed +90 mV (265 cochleae). This threshold was determined based on the average number of measurements in the healthy cochleae.[14]

Endolymph sampling was performed as follows. For each mouse, a tiny hole was created in the bony wall in the first turn of the cochlea to expose a small part of the spiral ligament. The tip of an electrode micropipette was placed on the surface of the perilymph in the hole and the potential was set to zero millivolts as the reference for subsequent recording. The electrode micropipette was then advanced through the spiral ligament and stria vascularis using a micromanipulator toward the scala media until the monitored potential increased to approximately +100 mV, a hallmark of the endolymph. After detecting the high potential, we further pushed the electrode micropipette forward by ∼50 μm so as to completely penetrate the stria vascularis. After confirmation of the stabilization of the potential value, we manually provided a 1 mL syringe connected to the electrode micropipette with a negative pressure representing ∼0.05 mL and slowly and carefully collected the endolymph. From each cochlea, 0.1–0.3 μL of endolymph was obtained.

This sample was then deposited in a Protein LoBind tube (0.5 mL) by applying a gentle positive pressure to the syringe connected to the pipette. In the two series of proteomic analyses (Figures 2, 3, and 4A), endolymph aliquots from 12 to 15 cochleae were gathered and combined in the tube (total volume: ∼2.5 μL). Afterward, 0.4 μL of the homogenized sample was taken and diluted in a requisite volume of ultrapure water (final volume: 100 μL), followed by protein concentration measurement (described in the following section). In the rest of the endolymph sample, a volume corresponding to 0.9 μg protein (∼2 μL) was subjected to LC-MS/MS analysis.

Similarly, in each series of western blotting analysis (Figures 4B and S3) endolymph aliquots obtained from 6 to 9 cochleae were gathered in a tube (total volume: ∼1.5 μL). A total of 0.4 μL of the combined sample was used for protein concentration measurement, whereas a volume containing 0.6 μg protein (∼1 μL) was subjected to immunoblotting.

Determination of protein concentrations of perilymph and endolymph samples

Before each biochemical assay, the protein concentration of the sample was determined by the Bradford method using spectrophotometry in accordance with the manufacturer's instruction (Protein Assay Kit; TaKaRa Bio, Shiga, Japan).[74]

In each series of experiments, 0.4 μL of the endolymph or perilymph sample gathered in a tube as mentioned above was diluted in a requisite volume of ultrapure water for a final volume of 100 μL. Then, this sample was mixed with 100 μL of Bradford Dye Reagent. The absorbance at 595 nm was measured by spectrophotometry to determine the protein concentrations.

Proteomic analysis of endolymph and perilymph

In each case, a sample of 0.9 μg protein was taken as mentioned above, reduced with 5 mM dithiothreitol (DTT), and heated at 95°C for 5 min to denature the proteins. The samples were then separated using precast 5–20% acrylamide SDS-PAGE gels (Fujifilm, Tokyo, Japan). Proteins in the gels were visualized by silver staining (Silver stain II kit; Wako, Tokyo, Japan).[75–77]

We performed two different series of proteomic analyses. In either case, mouse samples were analyzed by the 'In-gel digestion' method[78] followed by peptide sequencing, as described below. The first series involved a comprehensive analysis of proteins present in the two lymph fluids. Endolymph and perilymph samples (0.9 μg protein for each) were migrated by 1 cm in a gel. In each lane, the stained portion was excised using a scalpel, and the gel block was cut into 1 mm^3 portions. In the second series, we focused on the differences in data patterns between endolymph and perilymph. When the endolymph and perilymph samples were electrophoresed using SDS-PAGE, two bands specific to the former were identified (Figure 4A). Two portions containing these bands in the endolymph lane and the corresponding portions in

the perilymph lane were extracted, and the four blocks were cut into approximately 1 mm^3 portions. The gel pieces were subjected to LS-MS/MS analysis using a previously described method.[79]

LC-MS/MS analyses

In each series of experiments, the gel pieces taken from the polyacrylamide gels used to analyze the endolymph and perilymph samples were destained according to the procedure prescribed by the manufacturer.[75–77] After the samples were shrunken in acetonitrile, the proteins were reduced with 10 mM dithiothreitol in 100 mM NH_4HCO_3 at 56°C for 30 min, followed by washing with acetonitrile. Proteins were alkylated with 55 mM iodoacetamide in 100 mM NH_4HCO_3 at room temperature for 30 min in the dark. The samples were dehydrated in acetonitrile, and then hydrated with 50 mM acetic acid containing 20 ng/uL sequencing grade trypsin at 4°C for 10 min. The solutions were neutralized with 100 mM NH_4HCO_3, and the protein was digested at 37°C overnight (final trypsin concentration: 2 ng/μL). The samples were subjected to LC-MS/MS analysis.

LC-MS/MS analyses were performed as previously described.[79] Briefly, the samples were separated at a flow rate of 300 nL/min on a nano HPLC capillary column (C18, 3 μm, 100 Å pore size, 75 μm i.d., and 120 mm length; Nikkyo Technos, Tokyo, Japan) for 120 min. The eluted peptides were introduced into a Q-Exactive Orbitrap mass spectrometer (Thermo Fisher Scientific) controlled by Xcalibur 4.2 and analyzed in a scan range of *m/z* 350–1,500 with a resolution of 70,000 at *m/z* 200 for MS1. Ions with peak intensities above 2.0e5 and charge states from 2+ to 7+ were subjected to MS/MS. In MS2, the ions were fragmented via higher-energy collision dissociation. The MS and MS/MS spectral data were analyzed and proteins in the sample were identified with product ion search algorithms by assigning peptides to the corresponding proteins using Proteome Discoverer 2.3 (Thermo Fisher Scientific). The search results were filtered using a q-value threshold of 0.01.

Based on these results, perilymph and endolymph proteins were categorized using the Database for Annotation, Visualization, and Integrated Discovery (DAVID) software (GOTERM_CC_DIRECT for cellular components and GOTERM_BP_DIRECT for biological process analysis).

We determined the criteria for extracting proteins that were more abundantly expressed in the endolymph than in the perilymph. In the first series of proteomic analysis, the threshold was set with the number of unique peptides ≥ 5 and the PSM ≥ 1.1 (Figure 3C; Table S3). In the second series, each protein under the criterion satisfied the three conditions; the difference in identified unique peptides between endolymph and perilymph exceeded four (i.e., endolymph's peptides – perilymph's peptides ≥ 4), coverage difference between the two lymph fluids exceeded 5% (i.e., $\geq 5\%$), the actual molecular weight fell in either the range of 160 ± 50 kDa or 35 ± 15 kDa. Note that 'coverage' indicates the percentage of the protein sequences covered by identified peptides.

In the case of guinea pigs, 0.9 μg of endolymph and perilymph samples, which were obtained from 8 cochlea and 1 cochlea, respectively, were analyzed with SDS-PAGE and silver staining with the same procedures as used for mouse samples.

Western blotting

Endolymph and perilymph samples were prepared from 6 to 9 cochleae and 2 cochleae, respectively, and the samples (0.6 μg for each) were subjected to western blotting as previously described.[80] Briefly, the proteins separated by SDS-PAGE were electrophoretically transferred onto polyvinylidene difluoride membranes (Hercules, CA, USA). The membranes were incubated with blocking solution for 1 h at room temperature and then overnight at 4°C in blocking solution containing a primary antibody against each of the following five proteins: A2M (dilution, 1: 2000, cat. #MA5-38211; Invitrogen, Waltham, MA, USA, RRID: AB_2898128), OPN (0.1 μg/mL, cat. #: AF808; biotechne, Minneapolis, MN, USA, RRID: AB_2194992), APOE (dilution, 1:2000, #AB947; Darmstadt, Germany, RRID: AB_2258475), APOD (dilution, 1:3000, #PA5-27386; Invitrogen, Waltham, MA, USA, RRID: AB_2544862), APOJ (0.1 μg/mL, # AF2747; biotechne, Minneapolis, MN, USA, RRID: AB_2083314). The blocking solution consisted of 10 mM Tris-HCl (pH 7.6), 150 mM NaCl, 5% (w/v) skim milk (Wako), and 0.1% (w/v) Tween 20 (Wako). The primary antibodies were probed with horseradish peroxidase (HRP)-conjugated anti-rabbit IgG (Jackson ImmunoResearch Laboratories, West Grove, PA, USA, RRID: AB_2307391). Signals were visualized using ECL Prime western Blotting Detection Reagents (Cytiva, Marlborough, MA, USA) and a Bio-Rad ChemiDoc XRS apparatus (Bio-Rad Laboratories, Hercules, CA, USA). Thereafter, all the membranes were treated with a stripping buffer (100 mM 2-methylethanol, 2% SDS, and 62.5 mM Tris, pH 6.8) at 65°C for 30 min to remove the reagents and antibodies,[81] followed by re-probing with anti-albumin antibody (dilution, 1: 2000, #ab207327; Abcam, Cambridge, England, RRID: AB_2755031) (Figure S3A).

Similarly, the samples of mouse endolymph, perilymph, and tissue lysate of kidney (0.6 μg) were analyzed by western blotting with an antibody specific to β-actin (Proteintech, IL, USA, RRID: AB_2687938) (Figure S3B).

Immunolabeling

Immunolabeling assays were performed as per a previously described method.[82,83] Briefly, the mice were euthanized with an overdose of anesthetic and subjected to immunolabeling experiments. The inner ears were dissected from these mice and fixed with 4% paraformaldehyde (PFA) for 2 h at 4°C, followed by decalcification in 10% EDTA for 24 h at 4°C. The cochlear samples were then dehydrated with 30% (w/v) sucrose for 1 h and frozen with optimum cutting temperature compound (Tissue-Tek; Sakura Finetechnology, Tokyo, Japan). Sections (10 μm) were cut using a cryostat and mounted onto APS-coated slides (Mastunami, Tokyo, Japan). Samples were permeabilized in 0.25% Triton X-100 dissolved in PBS (Wako, Osaka, Japan) for 60 min at room temperature. After being treated with 0.5% blocking reagent (Roche Molecular Biochemicals, Indianapolis, IN, USA) for 1 h, the samples were incubated with an anti-A2M antibody (Abcam RRID: AB_879541) (rabbit; 1:500 dilution) overnight at 4°C. After washing three times with PBS, the samples were treated with Alexa Fluor 568-conjugated secondary

antibody (Thermo Fisher Scientific, Grand Island, NY, USA, RRID: AB_143157) (rabbit; 1:500 dilution) for 1 h at room temperature and then stained with DAPI (Thermo Fisher Scientific, 1:1000 dilution) for 30 min at room temperature. After washing three times with PBS, the samples were mounted onto glass slides with ProLong Glass Antifade Mountant (Thermo Fisher Scientific, Grand Island, NY, USA). Finally, fluorescent images were obtained using a Zeiss LSM 880 with an Airyscan confocal microscope (Carl Zeiss, Jena, Germany).

Quality evaluation of the antibody against A2M

HEK cells were transfected with a miniVec that had myc-tagged A2M cDNA (Vector Builder, Kanagawa, Japan). Untransfected cells were used as controls. These two series of cell lysates were analyzed by western blotting using an antibody against A2M or the antibody against myc (Proteintech Rosemont, IL, USA, RRID: AB_2148585). In immunolabeling assays, cells transfected with or without A2M cDNA were reacted with two antibodies against A2M and myc, and probed with Alexa Fluor 568-conjugated secondary antibody (Thermo Fisher Scientific) and Alexa Fluor 488-conjugated secondary antibody (Abcam, RRID: AB_2630356), respectively. The results are shown in Figure S4.

Reverse transcription PCR (RT-PCR)

Total RNA (1 μg) extracted from a whole adult cochlea using PureLink RNA Mini Kit (#12183018A, Thermo Fisher Scientific) was reverse-transcribed with PrimeScript 1st strand cDNA synthesis mix (#6215A, Takara bio). Synthesized cDNA and Ex Premier DNA polymerase (#RR371A, Takara) were combined with primers as follows: A2M -(product length 453 bp), 5′-TCTCACAATGCCCTACTCCG-3′ (sense) and 5′- GCTC GGGCAGATTCCTCTAC-3′ (antisense). PCR was performed using C1000 Touch Thermal Cycler (Bio-Rad) with the following reaction parameters: 2 min at 95°C, 34 cycles of 10 s at 95°C, 15 s at 60°C, 20 s at 68°C, followed by 5 min at 68°C. In addition, cDNA was synthesized from total RNA of liver tissue (1 μg) in a mouse of embryonic 18.5 days. Liver cDNA was used as a positive control, and a sample solution containing no cDNA was used as a negative control.

Auditory brainstem response (ABR) measurements

The ABR of 8 mice at 5 weeks of age was measured in accordance with our previous protocol[8] (Figure S5). The anesthetized mice were placed in the prone position in a soundproofed booth that was both acoustically and electrically shielded (Acoustic Systems Englewood, CO, USA). ABR was measured and recorded using a customized analysis platform (RZ6 Processor and BioSigRZ version 5.7.6 RRID: SCR_014820, respectively; Tucker-Davis Technologies, Alachua, FL, USA). In each animal, subdermal needle electrodes were inserted at the vertex, under the pinnae of the left ear, and under the pinnae of the contralateral ear (ground). Cos2-gated 1-ms tone burst stimuli (21/s, alternating polarity) of 4, 8, 16, or 32 kHz containing a 0.1-ms rising phase, a 0.8-ms duration phase, and a 0.1-ms falling phase were provided to the test ear by a closed-field speaker (MF-1; Tucker-Davis Technologies). The brainstem responses were processed with a bandpass filter (0.3–5 kHz) and averaged with 200–500 artifact-free responses per waveform.

For each stimulus frequency, the intensity was initially set to 90 dB SPL and subsequently reduced in 5-dB steps to a pressure level that no longer induced a discernable waveform. The auditory thresholds were determined by visual inspection of the stacked waveforms at the lowest stimulus level. ABR measurements were repeated when the threshold response was unclear.

QUANTIFICATION AND STATISTICAL ANALYSIS

Data shown in Figure 3A are expressed as the mean ± standard deviation (SD). Two-tailed Student's t-tests were used for comparisons between the two groups. Differences between groups with $p < 0.05$ were considered statistically significant. Microsoft Excel 2019 (Microsoft, Seattle, WA, USA) was used to calculate statistical parameters. The details are described in Figure 3A legends, Results section and method details in STAR Methods section. Data shown in Figure S5 are expressed as the mean ± standard error of the mean (SEM). The details are described in Figure S5 legends.